Microstructure and mechanical properties of friction welded carbon steel (EN24) and nickel-based superalloy (IN718)

V.T. Gaikwad[1,2], *M.K. Mishra*[1], *V.D. Hiwarkar*[2], *and R.K.P. Singh*[1]

1) Kalyani Centre for Technology and Innovation, Bharat Forge Limited, Pune 411036, India
2) Department of Materials Engineering, Defense Institute of Advance Technology, Pune 411025, India

Abstract: Continuous-drive rotary friction welding was performed to join cylindrical specimens of carbon steel (EN24) and nickel-based superalloy (IN718), and the microstructures of three distinct weld zones—the weld interface (WI)/thermo-mechanically affected zone (TMAZ), the heat-affected zone (HAZ), and the base metal—were examined. The joint was observed to be free of defects but featured uneven flash formation. Electron backscatter diffraction (EBSD) analysis showed substantial changes in high-angle grain boundaries, low-angle grain boundaries, and twin boundaries in the TMAZ and HAZ. Moreover, significant refinement in grain size (2–5 μm) was observed at the WI/TMAZ with reference to the base metal. The possible causes of these are discussed. The microhardness profile across the welded joint shows variation in hardness. The changes in hardness are ascribed to grain refinement, phase transformation, and the dissolution of strengthening precipitates. The tensile test results reveal that a joint efficiency of 100% can be achieved using this method.

1. Introduction

Friction welding (FW) is an economical and environment-friendly solid-state joining process that is applied to join similar as well as dissimilar ferrous and nonferrous materials [1]. In this technique, under pressure, relative motion is introduced between the contact surfaces, leading to an increase in the interface temperature due to frictional heat. After the appropriate temperature is attained, rotational motion is stopped, and forging pressure is exerted followed by self-cooling [2]. The microstructure and the subsequent mechanical properties of friction welded joints are influenced by the applied pressure, friction and upset time, and rotational speed. Among recently introduced joining techniques, FW is attractive because of its lower cycle time, higher productivity, and better product quality [3].

To reduce cost, the properties of two different materials are combined for many engineering applications. Joints of carbon steel and nickel-based superalloy are used in the aerospace, automobile, shipping, and petrochemical industries [4−5]. The literature shows that FW has been effectively applied to join dissimilar materials, such as austenitic stainless steels to carbon steels [6−8], nickel-based superal-

loys with titanium alloys [9], and titanium alloys with stainless steel [10]. Moreover, some researchers have used this technique to join similar materials such as carbon steels, aluminum alloys, and nickel-based superalloys [1,11−13]. Sahin *et al*. [13] joined AISI 1040 steel and reported grain size refinement at weld interface (WI), which could be favorable for the improvement of tensile strength and hardness of weld joint. Anitha *et al*. [14] observed that with increasing rotational speed and friction pressure, grain refinement occurred due to the enhancement of dynamic recrystallization (DRX). Khidhir and Baban [15] achieved 90% joint efficiency (discussed in Section 3.3.2) in joining AISI 1045 medium-carbon steel and AISI 316L austenitic stainless steel by FW methods. However, Kimur *et al*. [16] obtained 100% joint efficiency by joining a superalloy and heat-resistant steel by varying FW parameters.

Using the regular fusion welding methods to join Inconel alloys is challenging because of the occurrence of porosity, inclusion, cracking, and microstructural segregation. This problem can be reduced by the FW technique [4,12]. Moreover, to further improve the weld joint strength of IN718 superalloy, post-weld heat treatment (PWHT) is suggested by Wang *et al*. [17]. Lalam *et al*. [5] observed that

🖄 Springer

PWHT is beneficial to improve the joint strength but deteriorates the fracture toughness due to the precipitation of complex phases such as Ni_3Al_4, Fe_3Mn_7, and $Al_{0.9}Ni_{1.1}$. Damodaram *et al.* [18] joined IN718 rods under different heat treatment conditions and studied the effect of PWHT on the microstructure and mechanical properties of the weld joint. They concluded that after FW, double aging cycles (heating to 720°C for 8 h followed by furnace cooling up to 620°C and holding at 620°C for 8 h followed by air cooling) was the best method to restore the parent material properties.

Though FW is a solid-state joining process, some researchers have reported its negative impact on the joining of some dissimilar materials. During the FW of carbon steel and stainless steel, Ma *et al.* [6] detected carbides layer consisting of CrC and $Cr_{23}C_6$ at the WI, which are detrimental to mechanical properties. Similarly, Paventhan *et al.* [7] observed the formation of intermetallics such as $Cr_{23}C_6$ and Cr_7C_3 at the WI of medium-carbon steel and austenitic stainless steel, which deteriorate the fatigue strength. However, Madhusudhan Reddy and Venkata Ramana [19] tried to insert a nickel interlayer between high-strength maraging steel and low-carbon (EN24) steel to reduce the formation of intermetallic phases. Despite the development of new technology and the rapid automation in the industries, the FW of dissimilar materials and its implementation on the industrial level are still challenging tasks to researchers.

Considering the reports on the FW of dissimilar carbon steel (EN24) and nickel-based superalloy (IN718) are limited, the objective of the current research is to examine the microstructural evolution during FW and investigate the mechanical properties of the welded joint at room temperature.

2. Experimental

EN24 steel and IN718 round bars were used as the base metal for FW. The diameter and length of each sample were 16 and 65 mm, respectively. The chemical compositions of both base metals are presented in Table 1. The EN24 steel rods were in annealed condition. Their microstructure consisted of spheroidite, i.e., sphere-like carbides in a ferrite matrix (Fig. 1(a)). As-received IN718 rods were solution-treated and aged. The microstructure of the IN718 consisted of strengthening precipitates and MC-type carbides in a γ (Ni) matrix (Fig. 1(b)). To eliminate the defect at the weld joint, the surface area of the joint was perfectly polished and then cleaned with acetone.

Friction welding was performed on a 120 KN upset force capacity continuous-drive FW machine (model FWT12), with all the FW process parameters precisely controlled by a computer numerical control system. The machine can operate with high precision and excellent repeatability, with spindle speed ranging from 800 to 2500 r/min. It can weld a maximum diameter of 32 mm. Welding was performed by holding the IN718 and EN24 samples in the rotating side and feeding side, respectively as shown in Fig. 2(a). Different trials were conducted by varying the friction pressure between 3000 and 7000 kPa, upset pressure between 6000 and 10000 kPa, and friction time between 2 and 10 s. The optimized parameters used for this study are presented in Table 2.

After the FW, metallographic specimens were cut using a wire electrical discharge machine along the transverse direction of the weld joint. The cut samples were prepared by polishing and chemically etching according to the standard metallographic procedures. To reveal the microstructure of

Table 1.   Chemical compositions of base metals   wt%

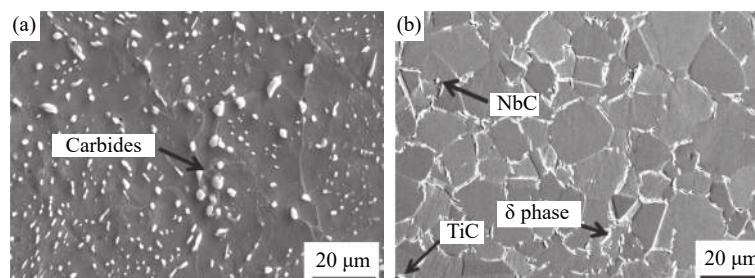| Metal	Ni	Cr	Nb	Mo	Ti	Al	C	Mn	Si	Cu	Fe
EN24	1.53	1.29	—	0.25	—	—	0.41	0.61	0.26	—	Bal.
IN718	53.60	17.82	5.05	3.01	0.66	0.45	0.08	—	—	0.04	16.91

Fig. 1.   Microstructures of base metals: (a) EN24; (b) IN718.

Table 2.   Friction welding parameters used for joining

Friction pressure / kPa	Friction time / s	Upset pressure / kPa	Upset time / s	Rotational speed / (r·min⁻¹)
5000	6	8000	3	1400

the IN718, Kalling's reagent consisting of 10 g $CuCl_2$, 200 mL HCl, and 200 mL ethanol was applied, whereas the EN24 side was etched using Nital. Microstructure analysis was performed using a scanning electron microscope equipped with a field emission gun. Chemical analysis was carried out using energy-dispersive spectroscopy (EDS). Samples for electron backscatter diffraction (EBSD) analysis were prepared by electro-polishing with an electrolyte of 200 mL perchloric acid, 100 mL 2-butoxy ethanol, and 700 mL ethanol. The parameters used for the electro-polishing were 24 V and 80 s. The EBSD scans were carried out at a step size of 0.4 µm using a Zeiss EVO18 scanning electron microscope. The grain boundary characteristics and grain size were determined using the Aztech HKL software. Tensile test specimens were prepared as per the ASTM E8 standard along the transverse direction to the weld joint, keeping the weld zone at the center of the gauge length. Tensile tests were carried out at ambient temperature, with a constant crosshead speed of 0.03 mm/s. Microhardness measurements were performed across the weld joint with a load of 500 g and dwell time of 10 s using a Zeiss microhardness testing machine.

3. Results and discussion

3.1. Microstructure of welded joint

The image of the welded joint is shown in Fig. 2(a). After careful visual inspection, the joint was confirmed to be without defects, indicating acceptable metallurgical properties. The reduction of axial length after FW is known as burn off, and the amount of material extruded is called flash [3].

As shown in Fig. 2(a), the total burn-off length was measured to be 9.0 mm; the reduction of lengths from WI to the EN24 side and IN718 side were 5.7 and 3.3 mm, respectively. The thermal conductivity of EN24 has been reported to be approximately 3.5 times higher than that of IN718 (IN718: 11.4 $W \cdot m^{-1} \cdot K^{-1}$ and EN24: 40.2 $W \cdot m^{-1} \cdot K^{-1}$) [4,20]. Thus, more heat is accumulated at the friction interface of the IN718 side than the EN24 side because of the lower thermal conductivity, which leads to uneven temperature distribution across the WI. Furthermore, at a high temperature, IN718 has a higher tensile strength compared with steel. Therefore, the EN24 experienced more deformation and extruded more material in terms of flash at the WI. The inverse pole figure (IPF) of the welded joint is presented in Fig. 2(b).

The weldment can be broadly divided into three zones: (1) the WI and/or thermo-mechanically affected zone (TMAZ), (2) the heat-affected zone (HAZ), and (3) the unaffected base metal at both sides. The WI thickness is very narrow, around 30 µm. The microstructure in this region consists of fine grains with an intermixture of EN24 and IN718 materials. The microstructural variations of the different zones on the EN24 alloy and IN718 are discussed in detail in Sections 3.1.1 and 3.1.2, respectively.

3.1.1. Microstructure of carbon steel (EN24) side

The microstructures in different zones of the rotary friction welded carbon steel (EN24) sides are presented in Fig. 3. The microstructure of the base metal consisted of spheroidite carbide particles distributed uniformly in the ferrite matrix as shown in Fig. 1(a). In the HAZ, deformed grains of fine pearlite and ferrite were observed (Fig. 3(a)). However, in the
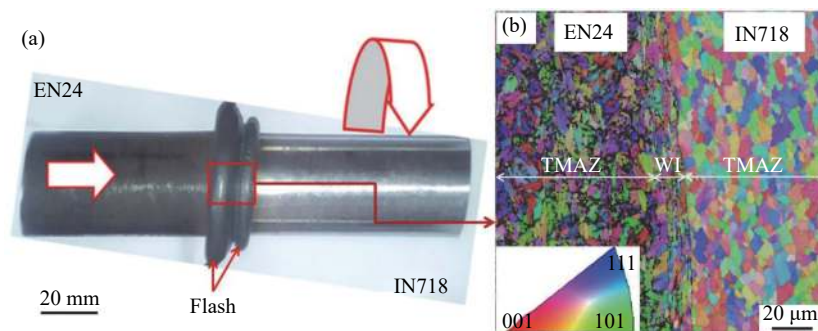

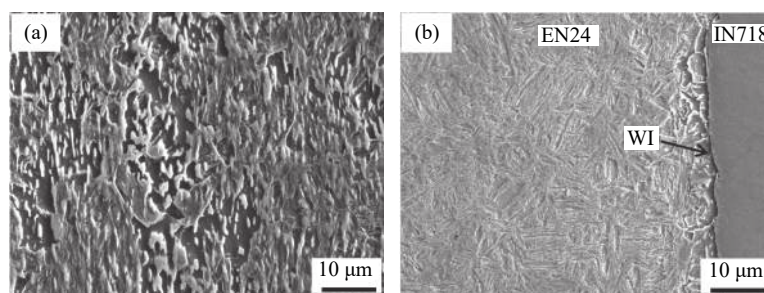**Fig. 2. Friction welded sample (a) and inverse pole figure of friction welded joint (b).**

Fig. 3. Scanning electron microscopy (SEM) micrographs of the EN24 side: (a) HAZ; (b) WI/TMAZ.

WI/TMAZ, a martensitic phase was observed (Fig. 3(b)). Due to friction, the temperature of the WI increased and reached the austenitic temperature range. When the rotational motion followed by upset pressure is stopped, self-quenching occurs in the bulk materials, resulting in the phase transformation of austenite to martensite [5,21].

3.1.2. Microstructure of Ni-based superalloy (IN718) side

The IN718 superalloy has good corrosion resistance and mechanical properties at elevated temperatures. The main strengthening precipitates for this alloy are γ′ [Ni₃(Al,Ti)] and γ″ (Ni₃Nb) [4]. Fig. 4 shows the microstructures of the IN718 side at various zones. The base metal (Figs. 4(a) and 4(a′)) comprised the γ matrix with fine γ′ and γ″ precipitates and a needle-shaped delta phase (δ) along grain boundaries. Moreover, titanium carbide and niobium carbide particles were dispersed in the matrix. The presence of these carbides and δ phase were confirmed by EDS point scanning (Figs. 4(a₁), 4(a₂), and 4(a₃)), and the weight percentages of elements are presented in Table 3.

Next to the base metal, elongated grains were present in the HAZ (Figs. 4(b) and 4(b′)). However, the WI/TMAZ showed a significant reduction in grain size due to the occurrence of DRX during welding, as indicated in Figs. 4(c) and 4(c′). A temperature beyond 850°C will result in the dissolution of γ′ and γ″ hard precipitates and δ phases in alloy 718 [12]. As observed from the SEM image, these precipitates were dissolved at the WI/TMAZ, depending on the temperature. To study the elemental distribution across the WI, an EDS line scan was performed, and the results are presented in Fig. 5. A significant change in element distribution, mainly for Fe, Ni, Nb, Cr, and Ti, was observed.

Furthermore, the lines corresponding to these elements present large scattering near WI, which is a mechanically mixed zone of two dissimilar materials (EN24 and IN718).

3.2. Electron backscatter diffraction

The IPF maps and misorientation distributions for the EN24 side are shown in Fig. 6. From Fig. 6(a), it can be understood that the base metal of the EN24 consisted of comparatively coarse grains. The fractions of HAGB and LAGB in the base metal were observed to be 0.04 and 0.96, respectively, and they drastically changed in the HAZ to 0.63 and
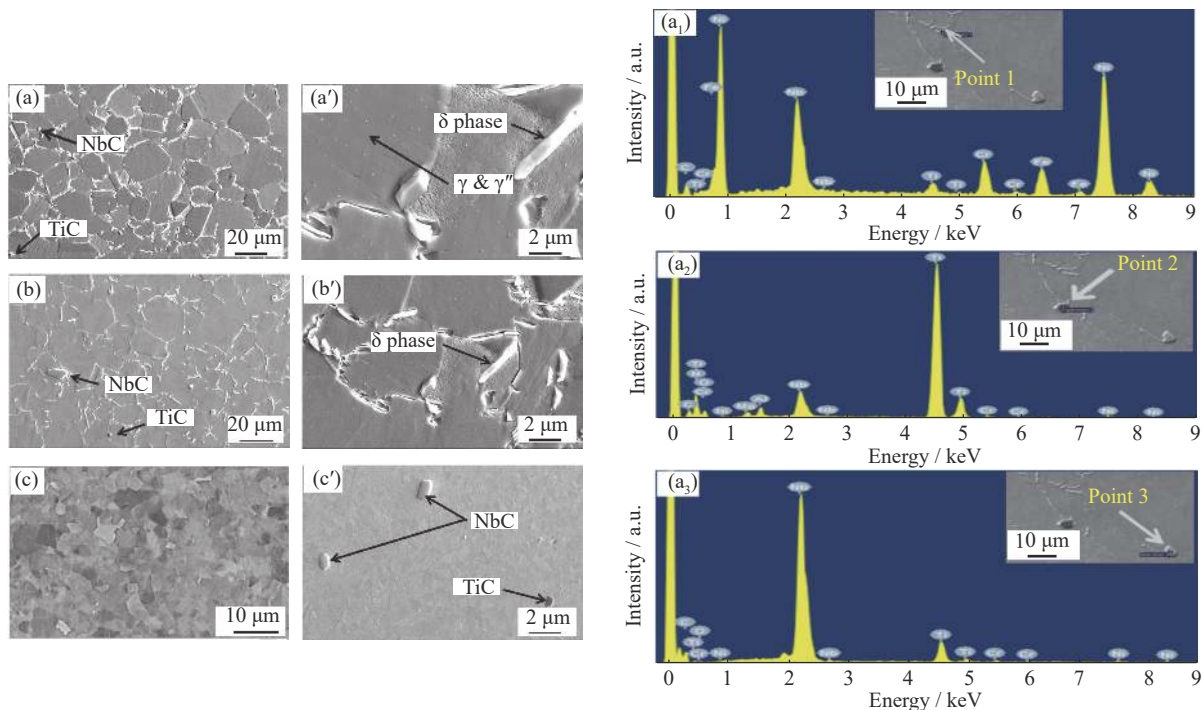

Fig. 4. SEM micrographs of the IN718 side: (a, a′) base metal; (b, b′) HAZ; (c, c′) WI/TMAZ (a′, b′, and c′ are magnified images of the base metal, HAZ, and WI, respectively). (a₁) EDS spectrum at point 1 (showing δ phase); (a₂) EDS spectrum at point 2 (showing TiC); (a₃) EDS spectrum at point 3 (showing NbC).

Table 3. Elemental distribution in δ phase and carbides wt%

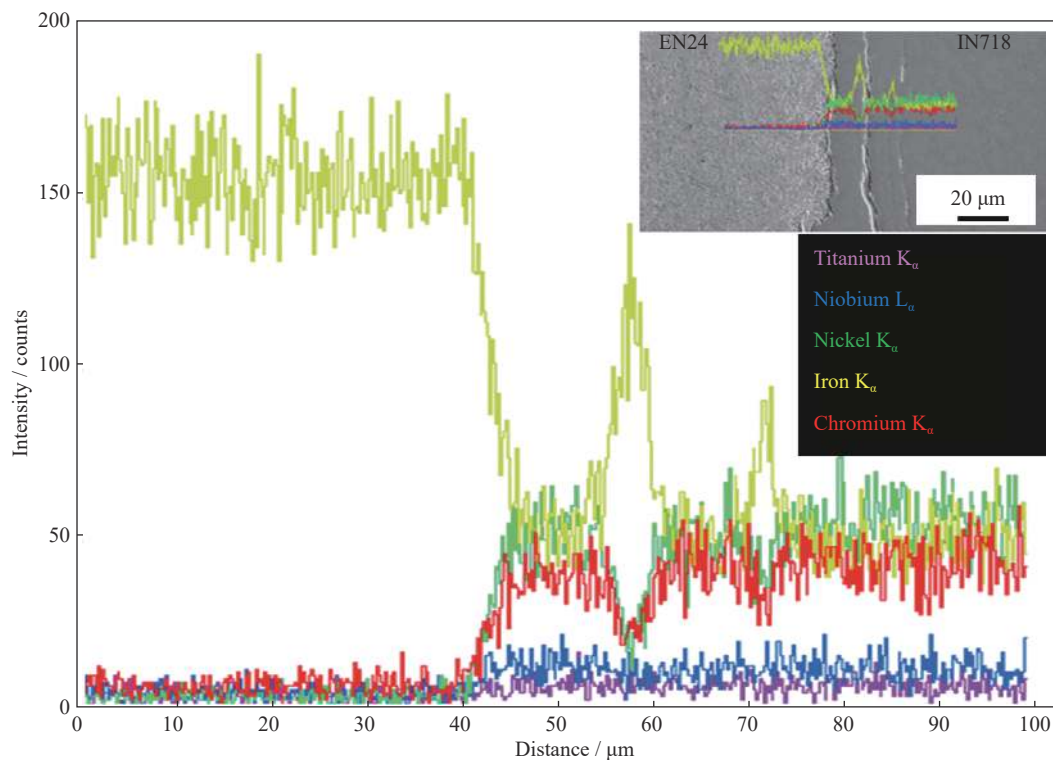| Point	C	Ti	Cr	Fe	Ni	Nb	N	O	Mg	Al	Total
1	13.21	1.51	6.28	7.17	52.13	19.69	—	—	—	—	100
2	7.39	45.41	0.56	—	0.83	8.27	20.01	15.64	0.79	1.1	100
3	30.39	7.22	0.73	—	1.05	57.48	—	3.13	—	—	100

Fig. 5. EDS line scan across the weld interface.

0.37, respectively. The increase in the HAGB and decrease in the LAGB are associated with DRX. It has been well established that DRX occurs during FW [12,22]. The critical strain for the recrystallization is provided by the plastic deformation produced by the upset force and the required temperature due to friction at the joining interface. However, the HAGB and LAGB fractions in the WI/TMAZ were found to be 0.36 and 0.64, respectively. The increase in the LAGB fraction compared with that of the HAZ may be due to the development of a martensite structure [23].

The IPF maps and misorientation distribution maps for the IN718 are given in Fig. 7. The base metal of the IN718 consisted of equiaxed grains with an average grain diameter of 20–22 μm. However, the HAZ showed slightly deformed grains whose size is close to that of the base-metal grains. Significant refinement in grain size up to 2–5 μm due to DRX was observed at the WI/TMAZ. From the misorientation distribution map, the HAGB and LAGB fractions were 0.94 and 0.06 in the IN718 base metal, respectively. However, in the HAZ, they were 0.78 and 0.22, respectively. Moreover, the WI showed a drastic change in grain boundary characteristics. The HAGB and LAGB fractions were observed to be 0.35 and 0.65, respectively.

The lower HAGB fraction and higher LAGB fraction in the HAZ and TMAZ compared with those in the base metal indicates that full static recrystallization did not take place in these zones. However, the percentage of twin boundaries (misorientation angle close to 60°) shows a reducing trend

from the base metal to the WI/TMAZ. The fractions of the twin boundaries in the base metal, HAZ, and WI/TMAZ are estimated to be around 0.18, 0.16, and 0.02, respectively. The large reduction in twin boundaries at the WI/TMAZ occurred because this region underwent severe plastic deformation at a high temperature. It has been reported that the ideal twin–matrix relationship is destroyed during the deformation, which decreases the fraction of the twin boundaries [24−25].

3.3. Mechanical properties
3.3.1. Microhardness

The microhardness variation across the WI is illustrated in Fig. 8. The variation of microhardness across the joint is related to the microstructure formed in the various welding zones. In the WI/TMAZ zone of the EN24 side, the peak microhardness value was found to be HV 635, which is significantly higher than that of the base metals. The increase in hardness is due to the combined effect of a martensitic structure formation and refinement in grain size (2–3 μm).

Grain refinement has been reported to occur due to DRX when the material experiences plastic deformation at high strain rates under elevated temperatures [26−27]. The hardness in the HAZ exhibited a decreasing trend from the WI toward the base metal, which is attributed to the formation of ferrite and pearlite in the microstructure.

Furthermore, the precipitates of the nickel-based superalloy (IN718) strengthened the material; the hardness of the material depends on the fractions of the γ' and γ'' precipitates
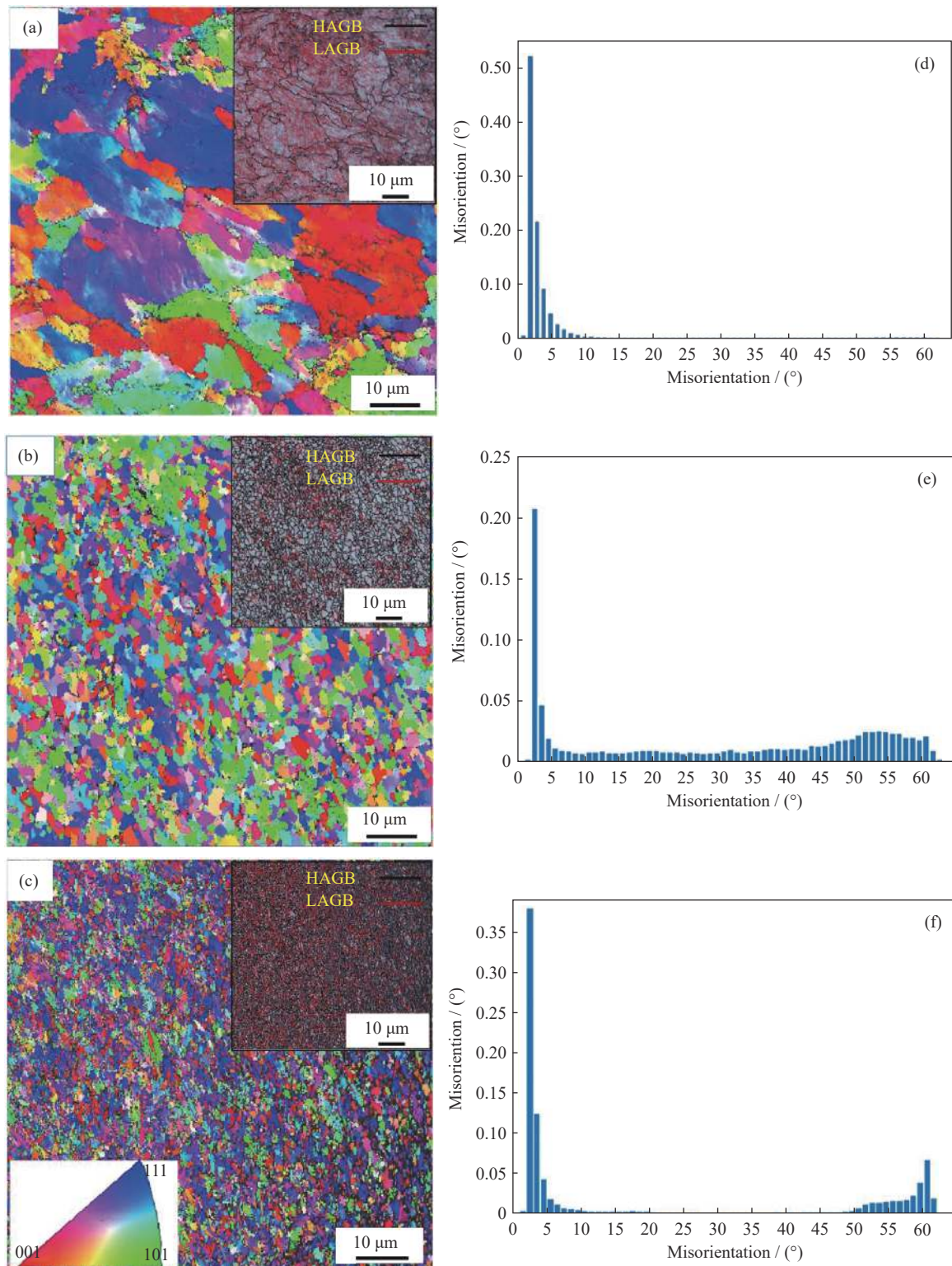
Fig. 6.   EBSD images for the EN24 side: inverse pole figure (IPF) maps (a–c) and misorientation distribution maps (d–f) for the base metal, HAZ, and WI/TMAZ, respectively. High-angle boundaries (HAGB, >15°); low-angle boundaries (LAGB, 2°–15°).

in the microstructure [4]. The WI/TMAZ and HAZ had a lower hardness compared with the base metal. This could be due to the dissolution of strengthening precipitates γ′ and γ″.

The base metal, which was not affected by heat and deformation, retained the hardness of the as-received parent metal, i.e., HV 440.
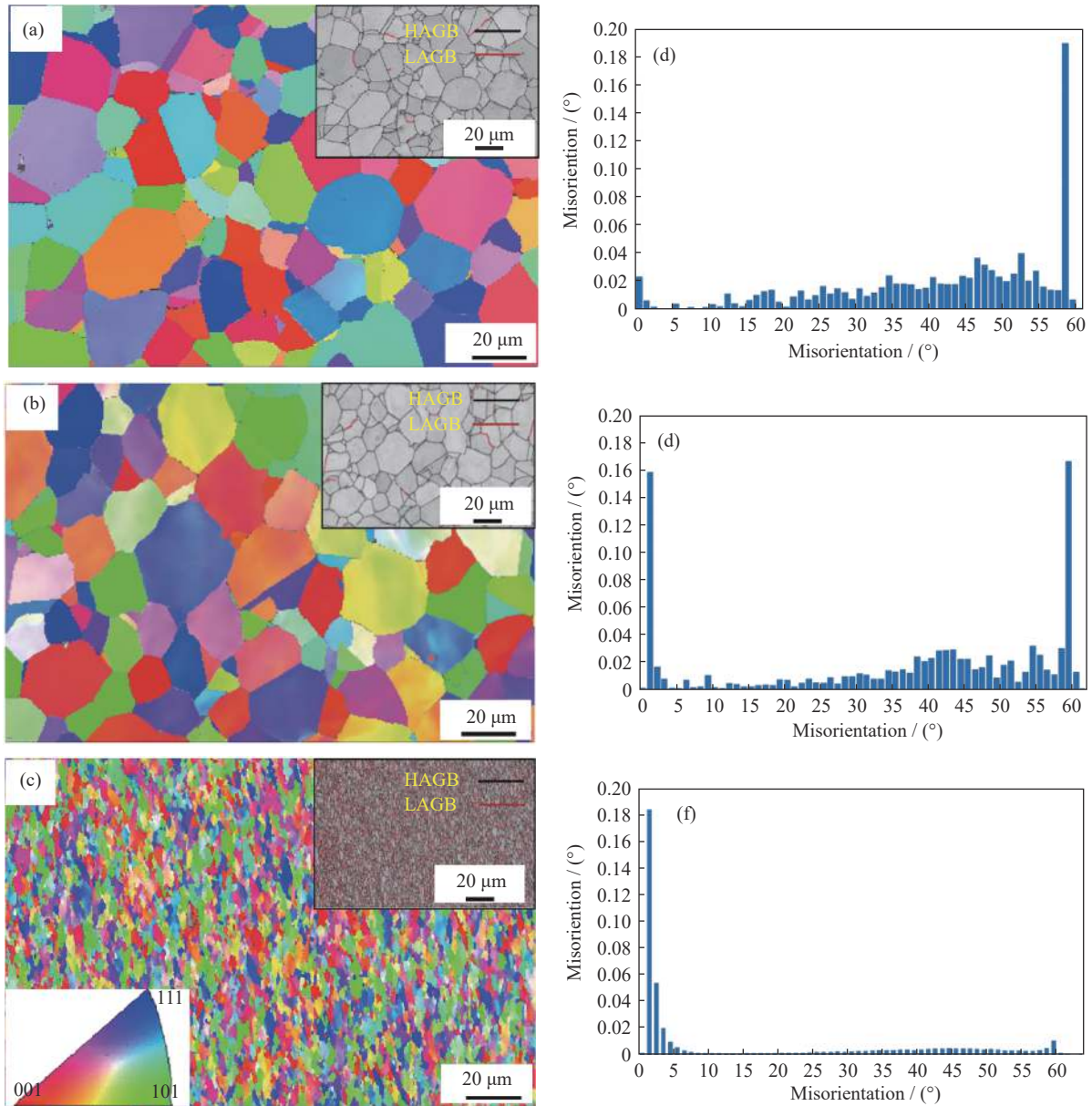
Fig. 7. EBSD images for the IN718 side: inverse pole figure (IPF) maps (a–c) and misorientation distribution maps (d–f) for the base metal, HAZ, WI/TMAZ, respectively. High-angle boundaries (HAGB, >15°); low-angle boundaries (LAGB, 2°–15°).

3.3.2. Tensile properties

The yield strength (YS), ultimate tensile strength (UTS), elongation, and joint efficiency of the welded joint are presented in Table 4. The weld samples showed YS that were almost equivalent to that of the EN24 base metal. However, the weld samples exhibited a lower ductility, which is due to the grain size refinement and martensite formation in the weld zone. Khidhir and Baban, [15] also reported lower ductility of the welded joint of dissimilar materials of AISI 1045 carbon steel and 316L austenitic stainless steel. The efficiency of the welded joint can be calculated as follows [15]:

$$\text{Joint efficiency } (\eta) = \frac{\text{Tensile strength of weld joint}}{\text{Tensile strength of soft materials (EN24 steel)}} \times 100\%$$

$$(1)$$

The UTS of the welded joint was around (772 ± 10.0) MPa, which shows a joint efficiency of ~100%. Therefore, the selected welding parameters are appropriate to generate friction heat and create plastic deformation at joints.

During tensile testing, failure occurred in weak or lower-hardness zones (base EN24). The SEM image of the fracture surface of the tensile-tested sample is shown in Fig. 9. The fractographs show the presence of dimples, indicating ductile failure.
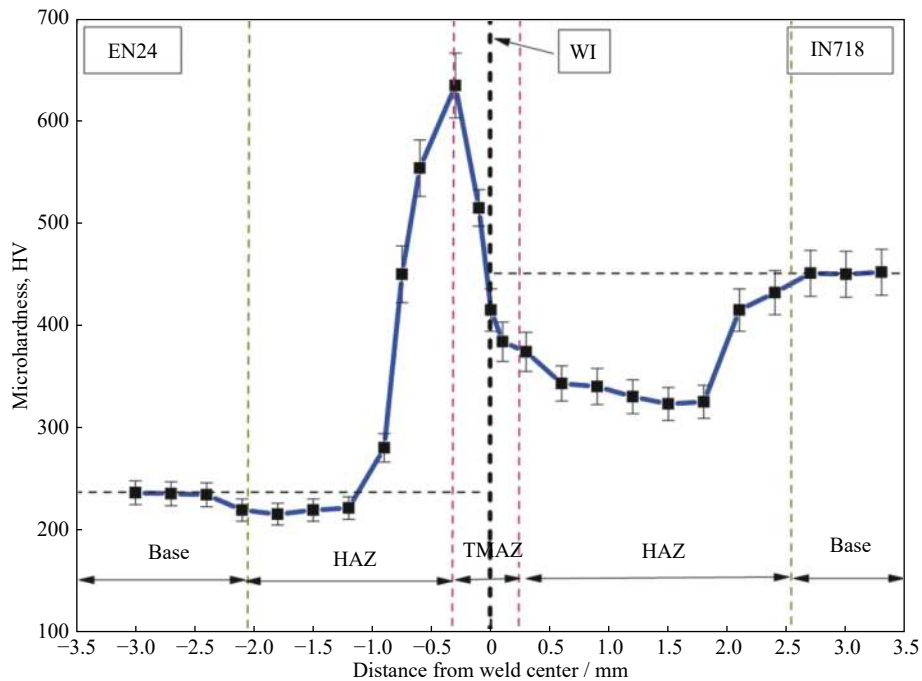
Fig. 8.   Microhardness distribution across the weld interface.

Table 4.   Tensile properties of base metals and weld samples

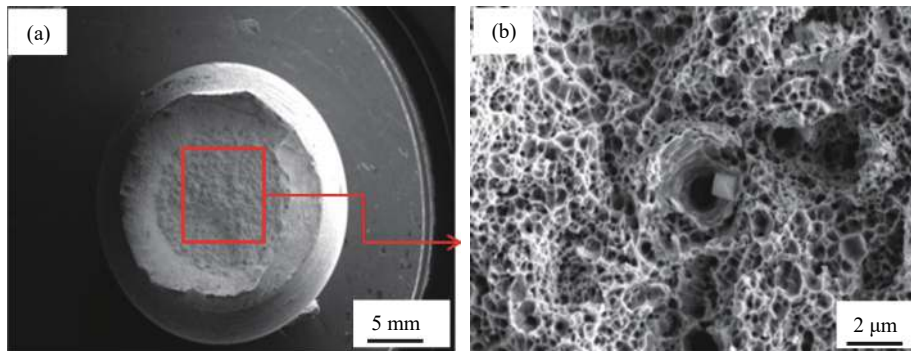| Sample	Yield strength (YS) / MPa	Ultimate tensile strength (UTS) / MPa	Elongation / %	Joint efficiency (η) / %
Base-EN24	675 ± 7.0	767 ± 15.0	22 ± 1.5	
Base-IN718	1188 ± 8.0	1374 ± 9.0	24 ± 3.0	
Weld sample	681 ± 5.0	772 ± 10.0	14.8 ± 1.0	~100.0

Fig. 9.   Fractographs of tensile fracture sample: (a) SEM image of failure sample; (b) magnified image.

4. Conclusions

The following conclusions can be drawn from the present work on the FW of dissimilar EN24 alloy steel and IN718 superalloy.

(1) The welded joint was observed to be free of defects, with the overall burn-off length being 9.0 mm. However, the flash width was uneven due to the difference in thermal conductivity and yield strength between the two metals.

(2) The EBSD results showed a significant refinement of grain size (2–5 μm) in the IN718 TMAZ. The grain bound-

ary characteristics of the WI/TMAZ and HAZ were different from that of the base metal due to the combined effect of heat and severe plastic deformation. Moreover, the fraction of twin boundaries in the WI was lower than that of the base metal, and this can be ascribed to the severe thermo-mechanical deformation.

(3) The hardness variation across the weld joint is attributed to grain refinement, phase transformation, and the presence of strengthening precipitates. The peak hardness (HV 635) was observed toward the TMAZ of the EN24 side, due to the formation of a martensite structure and grain refine-

ment, while the TMAZ of the IN718 exhibited a lower hardness (HV 385) compared with that of the base metal due to dissolution of strengthening precipitates. Moreover, the UTS of the welded joint was equivalent to that of the EN24 base metal.

Acknowledgement

References

[1] W. Cai, G. Daehn, A. Vivek, J.L. Li, H. Khan, R.S. Mishra, and M. Komarasamy, A state-of-the-art review on solid-state metal joining, *J. Manuf. Sci. Eng.*, 141(2019), No. 3, art. No. 031012.

[2] W.Y. Li, A. Vairis, M. Preuss, and T.J. Ma, Linear and rotary friction welding review, *Int. Mater. Rev.*, 61(2016), No. 2, p. 71.

[3] American Welding Society, American National Standard ANSI/AWS C6.1-89 (R2009), *Recommended Practice for Friction Welding*, American National Standards Institute, Miami, 1989.

[4] M.J. Donachie and S.J. Donachie, *Superalloys: A Technical Guide*, ASM international, 2nd ed, Materials Park, 2002, p. 245.

[5] S.V. Lalam, G.M. Reddy, T. Mohandas, M. Kamaraj, and B.S. Murty, Continuous drive friction welding of Inconel 718 and EN24 dissimilar metal combination, *Mater. Sci. Technol.*, 25(2009), No. 7, p. 851.

[6] H. Ma, G.L. Qin, P.H. Geng, F. Li, B.L. Fu, and X.M. Meng, Microstructure characterization and properties of carbon steel to stainless steel dissimilar metal joint made by friction welding, *Mater. Des.*, 86(2015), p. 587.

[7] R. Paventhan, P.R. Lakshminarayanan, and V. Balasubramanian, Fatigue behaviour of friction welded medium carbon steel and austenitic stainless steel dissimilar joints, *Mater. Des.*, 32(2011), No. 4, p. 1888.

[8] H. Ma, G.L. Qin, P.H. Geng, F. Li, X.G. Meng, and B.L. Fu, Effect of post-weld heat treatment on friction welded joint of carbon steel to stainless steel, *J. Mater. Process. Technol.*, 227(2016), p. 24.

[9] P. Wanjara, J. Gholipour, K. Watanabe, K. Nezaki, Y. Tian, and M. Brochu, Linear friction welding of IN718 to Ti6Al4V, *Mater. Sci. Forum*, 879(2017), p. 2072.

[10] M. Cheepu and W.S. Che, Characterization of microstructure and interface reactions in friction welded bimetallic joints of titanium to 304 stainless steel using nickel interlayer, *Trans. Indian Inst. Met.*, 72(2019), No. 6, p. 1597.

[11] Z.W. Huang, H.Y. Li., M. Pruess, M. Karadge, P. Bowen, S. Bray, and G. Baxter, Inertia friction welding dissimilar nickel-based superalloys alloy 720LI to IN718, *Metall. Mater. Trans. A*, 38(2007), No. 7, p. 1608.

[12] R. Damodaram, S.G.S. Raman, and K.P. Rao, Microstructure and mechanical properties of friction welded alloy 718, *Mater. Sci. Eng. A*, 560(2013), p. 781.

[13] M. Sahin, H.E. Akata, and T. Gulmez, Characterization of mechanical properties in AISI 1040 parts welded by friction welding, *Mater. Charact.*, 58(2007), No. 10, p. 1033.

[14] P. Anitha, M.C. Majumder, V. Saravanan, and S. Rajakumar, Microstructural characterization and mechanical properties of friction-welded IN718 and SS410 dissimilar joint, *Metall. Microstruct. Anal.*, 87(2018), No. 3, p. 277.

[15] G.I. Khidhir and S.A. Baban, Efficiency of dissimilar friction welded 1045 medium carbon steel and 316L austenitic stainless steel joints, *J. Mater. Res. Technol.*, 8(2019), No. 2, p. 1926.

[16] M. Kimur, K. Nakashima, M. Kusaka, K. Kaizu, Y. Nakatani, and M. Takahashi, Joining phenomena and tensile strength of joint between Ni-based superalloy and heat-resistant steel by friction welding, *Int. J. Adv. Manuf. Technol.*, 103(2019), No. 1-4, p. 1297.

[17] H.J. Wang, K. Ikeuchi, M. Aritoshi, M. Takahashi, and A. Ikeda, Joint strength of Inconel 718 alloy and its improvement by post-weld heat treatment–joint performance and its controlling factors in friction welding of Inconel 718 alloy, *Weld. Int.*, 23(2009), No. 9, p. 679.

[18] R. Damodaram, S. Ganesh Sundara Raman, and K. Prasad Rao, Effect of post-weld heat treatments on microstructure and mechanical properties of friction welded alloy 718 joints, *Mater. Des.*, 53(2014), p. 954.

[19] G. Madhusudhan Reddy and P. Venkata Ramana, Role of nickel as an interlayer in dissimilar metal friction welding of maraging steel to low alloy steel, *J. Mater. Process. Technol.*, 212(2012), No. 1, p. 66.

[20] J. Woolman and R.A. Mottram, *The Mechanical and Physical Properties of the British Standard EN steels (B.S. 970-1955): En 21 to En 39*, Elsevier, 1966, p. 87.

[21] V.T. Gaikwad, V.D. Hiwarkar, V.P. Pawar, and R.K.P. Singh, Microstructure characterization and evaluation of mechanical properties for friction welded En-24 alloy steel, [in] *Materials Science & Technology (MS&T)2018*, Columbus, 2018, p. 822.

[22] Y. Wang, W.Z. Shao, L. Zhen, and X.M. Zhang, Microstructure evolution during dynamic recrystallization of hot deformed superalloy 718, *Mater. Sci. Eng. A*, 486(2008), No. 1-2, p. 321.

[23] Y.X. Zheng, F.N. Wang, C.R. Li, Y.L. Li, J. Cheng, and R.F. Cao, Effect of microstructure and precipitates on mechanical properties of Cr–Mo–V alloy steel with different austenitizing temperatures, *ISIJ Int.*, 58(2018), No. 6, p. 1126.

[24] M.K. Mishra, A.G. Rao, I. Balasundar, B.P. Kashyap, and N. Prabhu, On the microstructure evolution in friction stir processed 2507 super duplex stainless steel and its effect on tensile behaviour at ambient and elevated temperatures, *Mater. Sci. Eng. A*, 719(2018), p. 82.

[25] J. Jeon, S. Mironov, Y.S. Sato, H. Kokawa, S.C.H. Park, and S. Hirano, Friction stir spot welding of single-crystal austenitic stainless steel, *Acta Mater.*, 59(2011), No. 20, p. 7439.

[26] V. Patel, W.Y. Li, A. Vairis, and V. Badheka, Recent development in friction stir processing as a solid - state grain refinement technique: microstructural evolution and property enhancement, *Crit. Rev. Solid State Mater. Sci.*, 44(2019), No. 5, p. 378.

[27] S.M. Aktarer, D.M. Sekban, T. Kucukomeroglu, and G. Purcek, Microstructure, mechanical properties and formability of friction stir welded dissimilar materials of IF-steel and 6061 Al alloy, *Int. J. Miner. Metall. Mater.*, 26(2019), No. 6, p. 722.